

# Chiral three-nucleon forces and neutron matter

K. Hebeler<sup>1,\*</sup> and A. Schwenk<sup>1,2,3,†</sup>

<sup>1</sup>*TRIUMF, 4004 Wesbrook Mall, Vancouver, BC, V6T 2A3, Canada*

<sup>2</sup>*ExtreMe Matter Institute EMMI, GSI Helmholtzzentrum für Schwerionenforschung GmbH, 64291 Darmstadt, Germany*

<sup>3</sup>*Institut für Kernphysik, Technische Universität Darmstadt, 64289 Darmstadt, Germany*

We calculate the properties of neutron matter and highlight the physics of chiral three-nucleon forces. For neutrons, only the long-range  $2\pi$ -exchange interactions of the leading chiral three-nucleon forces contribute, and we derive density-dependent two-body interactions by summing the third particle over occupied states in the Fermi sea. Our results for the energy suggest that neutron matter is perturbative at nuclear densities. We study in detail the theoretical uncertainties of the neutron matter energy, provide constraints for the symmetry energy and its density dependence, and explore the impact of chiral three-nucleon forces on the  $S$ -wave superfluid pairing gap.

PACS numbers: 21.65.Cd, 21.30.-x, 21.60.Jz

## I. INTRODUCTION

The physics of neutron matter ranges over exciting extremes: from universal properties at low densities [1, 2] that can be probed in experiments with ultracold atoms [3]; to using neutron matter properties at nuclear densities to guide the development of a universal density functional [4, 5] and to constrain the physics of neutron-rich nuclei; to higher densities involved in the structure of neutron stars [6]. In the theory of nuclear matter, recent advances [7, 8] are based on systematic chiral effective field theory (EFT) interactions [9, 10] combined with a renormalization group (RG) evolution to low momenta [11, 12]. This evolution improves the convergence of many-body calculations [7, 13, 14] and the nuclear matter energy shows saturation with controlled uncertainties [8]. In this paper, we extend these developments to neutron matter with a focus on three-nucleon (3N) forces.

Our studies are based on evolved nucleon-nucleon (NN) interactions at next-to-next-to-next-to-leading order ( $N^3$ LO) [15, 16] and on the leading  $N^2$ LO 3N forces [17, 18]. In Sect. II, we show that only the long-range  $2\pi$ -exchange 3N interactions contribute in pure neutron matter. We then construct density-dependent two-body interactions  $\bar{V}_{3N}$  by summing the third particle over occupied states in the Fermi sea. Effective interactions of this sort have been studied in the past using 3N potential models and approximate treatments (see for example, Refs. [19, 20]). We derive a general operator and momentum structure of  $\bar{V}_{3N}$  and analyze the partial-wave contributions and the density dependence of  $\bar{V}_{3N}$ . This provides insights to the role of chiral 3N forces in neutron matter.

In Sect. III, we apply  $\bar{V}_{3N}$  to calculate the properties of neutron matter as a function of Fermi momentum  $k_F$  (or the density  $\rho = k_F^3/(3\pi^2)$ ) based on a loop expansion

around the Hartree-Fock energy. Our second-order results for the energy suggest that neutron matter is perturbative at nuclear densities, where  $N^2$ LO 3N forces provide a repulsive contribution. We study in detail the theoretical uncertainties of the neutron matter energy and find that the uncertainty in the  $c_3$  coefficient of 3N forces dominates. Other recent neutron matter calculations lie within the resulting energy band. In addition, the energy band provides constraints for the symmetry energy and its density dependence. Finally, we study the impact of chiral 3N forces on the  $^1S_0$  superfluid pairing gap at the BCS level. We conclude and give an outlook in Sect. IV.

## II. THREE-NUCLEON FORCES AS DENSITY-DEPENDENT TWO-BODY INTERACTIONS

Nuclear forces depend on a resolution scale, which is generally determined by a momentum cutoff  $\Lambda$ , and are given by an effective theory for scale-dependent two- and corresponding many-nucleon interactions [9–11, 21]:

$$H(\Lambda) = T + V_{NN}(\Lambda) + V_{3N}(\Lambda) + V_{4N}(\Lambda) + \dots \quad (1)$$

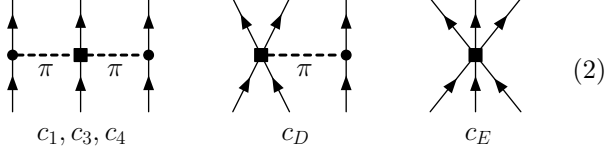
Our calculations are based on chiral EFT interactions. We start from the  $N^3$ LO NN potential ( $\Lambda = 500$  MeV) of Ref. [15] and use the RG to evolve this NN potential to low-momentum interactions  $V_{\text{low } k}$  with a smooth  $n_{\text{exp}} = 4$  regulator with  $\Lambda = 1.8 - 2.8 \text{ fm}^{-1}$  [12, 22]. This evolution softens the short-range repulsion and short-range tensor components of the initial chiral interaction [7, 23]. Based on the universality of  $V_{\text{low } k}$  [8, 12], we do not expect large differences starting from different  $N^3$ LO potentials.

In chiral EFT without explicit Deltas, 3N forces start at  $N^2$ LO and contain a long-range  $2\pi$ -exchange part  $V_c$ , an intermediate-range  $1\pi$ -exchange part  $V_D$  and a short-

\*E-mail: hebeler@triumf.ca

†E-mail: schwenk@triumf.ca

range contact interaction  $V_E$  [17, 18]:



The  $2\pi$ -exchange interaction is given by

$$V_c = \frac{1}{2} \left( \frac{g_A}{2f_\pi} \right)^2 \sum_{i \neq j \neq k} \frac{(\boldsymbol{\sigma}_i \cdot \mathbf{q}_i)(\boldsymbol{\sigma}_j \cdot \mathbf{q}_j)}{(q_i^2 + m_\pi^2)(q_j^2 + m_\pi^2)} F_{ijk}^{\alpha\beta} \tau_i^\alpha \tau_j^\beta, \quad (3)$$

where  $\mathbf{q}_i = \mathbf{k}'_i - \mathbf{k}_i$  denotes the difference of initial and final nucleon momenta ( $i, j$  and  $k = 1, 2, 3$ ) and

$$F_{ijk}^{\alpha\beta} = \delta^{\alpha\beta} \left[ -\frac{4c_1 m_\pi^2}{f_\pi^2} + \frac{2c_3}{f_\pi^2} \mathbf{q}_i \cdot \mathbf{q}_j \right] + \sum_\gamma \frac{c_4}{f_\pi^2} \epsilon^{\alpha\beta\gamma} \tau_k^\gamma \boldsymbol{\sigma}_k \cdot (\mathbf{q}_i \times \mathbf{q}_j), \quad (4)$$

while the  $1\pi$ -exchange and contact interactions are given respectively by

$$V_D = -\frac{g_A}{8f_\pi^2} \frac{c_D}{f_\pi^2 \Lambda_\chi} \sum_{i \neq j \neq k} \frac{\boldsymbol{\sigma}_j \cdot \mathbf{q}_j}{q_j^2 + m_\pi^2} (\boldsymbol{\tau}_i \cdot \boldsymbol{\tau}_j) (\boldsymbol{\sigma}_i \cdot \mathbf{q}_j), \quad (5)$$

$$V_E = \frac{c_E}{2f_\pi^4 \Lambda_\chi} \sum_{j \neq k} (\boldsymbol{\tau}_j \cdot \boldsymbol{\tau}_k), \quad (6)$$

with  $g_A = 1.29$ ,  $f_\pi = 92.4$  MeV,  $m_\pi = 138.04$  MeV and  $\Lambda_\chi = 700$  MeV. For 3N interactions, we use a smooth regulator as in Ref. [8],

$$f_R(p, q) = \exp \left[ -\frac{(p^2 + 3q^2/4)^2}{\Lambda_{3NF}^4} \right], \quad (7)$$

with a 3N cutoff  $\Lambda_{3NF}$  that is allowed to vary independently of the NN cutoff and probes short-range three-body physics. Here,  $p$  and  $q$  are initial Jacobi momenta (the final Jacobi momenta are denoted by  $p'$  and  $q'$ ). The exchange terms of the 3N force are included by means of the antisymmetrizer

$$\mathcal{A}_{123} = (1 + P_{12}P_{23} + P_{13}P_{23})(1 - P_{23}), \quad (8)$$

$$= 1 - P_{12} - P_{13} - P_{23} + P_{12}P_{23} + P_{13}P_{23}, \quad (9)$$

where  $P_{ij}$  is the exchange operator for spin, isospin and momenta of nucleons  $i$  and  $j$ . The regulator  $f_R(p, q)$  is totally symmetric when expressed in the nucleon momenta  $\mathbf{k}_i$ , and thus the direct and exchange terms contain the same regulator.

In this work, we take the N<sup>2</sup>LO 3N forces as a truncated basis for low-momentum 3N interactions and assume that the  $c_i$  coefficients of the long-range  $2\pi$ -exchange part  $V_c$  are not modified by the RG evolution. This follows the strategy adapted in Refs. [7, 8, 24], until it will be possible to evolve many-body forces in

momentum space starting from chiral EFT. For chiral low-momentum interactions, the  $c_D$  and  $c_E$  couplings have been fit for various cutoffs to the <sup>3</sup>H binding energy and the <sup>4</sup>He radius in Ref. [8]. However, as will be shown in the following, in pure neutron matter only the  $c_1$  and  $c_3$  terms of the  $2\pi$ -exchange part  $V_c$  contribute, so that the leading low-momentum three-neutron interactions will not depend on the shorter-range parts. Since the  $c_D$  and  $c_E$  couplings do not enter in neutron matter, we take for the  $c_i$  coefficients the consistent values used in the N<sup>3</sup>LO NN potential of Ref. [15], in particular  $c_1 = -0.81$  GeV<sup>-1</sup> and  $c_3 = -3.2$  GeV<sup>-1</sup>.

In addition, we will estimate the uncertainties of the two assumptions we have made for 3N forces. First, we will vary the cutoff to probe the sensitivity to neglected short-range many-body interactions and to the completeness of the many-body calculation. Second, we will study the dependence of our results on the choice of the  $c_i$  coefficients within their theoretical uncertainties in Sect. III D.

### A. Chiral 3N forces in neutron matter

Neutron matter presents a very interesting system, because only certain parts of the N<sup>2</sup>LO 3N forces contribute (see, for instance, Ref. [25]). First, the contact interaction  $V_E$  vanishes between antisymmetrized states, because three neutrons cannot interact in relative  $S$ -wave states due to the Pauli principle.

Second, the antisymmetrized  $1\pi$ -exchange part  $V_D$  vanishes due to the particular spin-momentum structure of this interaction. With  $\boldsymbol{\tau}_i \cdot \boldsymbol{\tau}_j = 1$  for neutrons, one has

$$\mathcal{A}_{123} V_D |_{nnn} \sim \mathcal{A}_{123} \sum_{i \neq j \neq k} \frac{\boldsymbol{\sigma}_j \cdot \mathbf{q}_j \boldsymbol{\sigma}_i \cdot \mathbf{q}_i}{q_j^2 + m_\pi^2}, \quad (10)$$

where in Eq. (10) and in the following the isospin exchange operator  $P_{ij}^\tau = 1$  in the antisymmetrizer. The sum over  $i \neq j \neq k$  can be grouped into three terms,  $\boldsymbol{\sigma}_1 \cdot \mathbf{q}_1 (\boldsymbol{\sigma}_2 + \boldsymbol{\sigma}_3) \cdot \mathbf{q}_1$ , and with 1 (23) replaced by 2 (13) and 3 (12). The first of these three terms is independent of the momenta of particles 2 and 3 and is nonvanishing only if the spin part of the wave function is symmetric under the exchange of the spins of particles 2 and 3. This implies  $P_{23} = 1$  and using the product representation of the antisymmetrizer, Eq. (8), leads to

$$\mathcal{A}_{123} \boldsymbol{\sigma}_1 \cdot \mathbf{q}_1 (\boldsymbol{\sigma}_2 + \boldsymbol{\sigma}_3) \cdot \mathbf{q}_1 = 0. \quad (11)$$

The other two terms in  $V_D$  vanish similarly. The physical reason for  $\mathcal{A}_{123} V_D |_{nnn} = 0$  is that the two particles interacting through the contact interaction  $c_D$  of Eq. (2) are required to be in a symmetric two-body spin state due to the structure  $\boldsymbol{\sigma}_i + \boldsymbol{\sigma}_j$  (because pion exchange couples to the sum of the spins), but the interaction does not depend on the momenta of these two particles, which means the momentum-space wave function will be symmetric. Therefore, the two particles cannot be in an overall antisymmetric state.

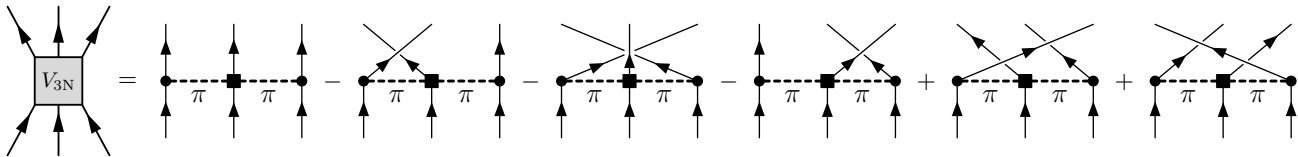


FIG. 1: Diagrammatic representation of the antisymmetrized  $N^2LO$  3N force in neutron matter. The  $c_4$  term in  $V_c$  and the shorter-range parts  $V_D$  and  $V_E$  vanish in neutron matter.

Finally, the  $c_4$  term in Eq. (4) of the  $2\pi$ -exchange part  $V_c$  does not contribute for neutrons, because of the isospin structure with  $\langle nnn | \boldsymbol{\tau}_1 \cdot (\boldsymbol{\tau}_2 \times \boldsymbol{\tau}_3) | nnn \rangle = 0$ . As a result, the  $N^2LO$  3N force in neutron matter is given by

$$\begin{aligned} \mathcal{A}_{123} V_{3N} |_{nnn} &= f_R(p', q') f_R(p, q) \frac{g_A^2}{4f_\pi^4} \mathcal{A}_{123} \\ &\times \sum_{i \neq j \neq k} \frac{(\boldsymbol{\sigma}_i \cdot \mathbf{q}_i)(\boldsymbol{\sigma}_j \cdot \mathbf{q}_j)}{(q_i^2 + m_\pi^2)(q_j^2 + m_\pi^2)} [-2c_1 m_\pi^2 + c_3 \mathbf{q}_i \cdot \mathbf{q}_j]. \end{aligned} \quad (12)$$

The direct, single- and double-exchange terms included in Eq. (12) are shown diagrammatically in Fig. 1. Since  $c_3$  is typically a factor 4 larger than  $c_1$  and because  $\mathbf{q}_i \cdot \mathbf{q}_j$  increases with density compared to  $m_\pi^2$  (for densities of interest  $q \sim k_F \sim 2m_\pi$ ), the  $N^2LO$  3N force in neutron matter is therefore dominated by the  $c_3$  contribution.

### B. Operator structure of $\bar{V}_{3N}$

Based on the  $N^2LO$  3N force, Eq. (12), we construct an antisymmetrized density-dependent two-body interaction  $\bar{V}_{3N}$  in neutron matter by summing the third particle over occupied states in the Fermi sea,

$$\bar{V}_{3N} = \text{Tr}_{\sigma_3} \int \frac{d\mathbf{k}_3}{(2\pi)^3} n_{\mathbf{k}_3} \mathcal{A}_{123} V_{3N} |_{nnn}, \quad (13)$$

where the trace is over the spin of the third particle and  $n_{\mathbf{k}}$  denotes the Fermi-Dirac distribution function at zero temperature,  $n_{\mathbf{k}} = \theta(k_F - |\mathbf{k}|)$ . The antisymmetrization in Eq. (13) can also be written in a more symmetric form using normalized and antisymmetrized three-body states,  $|123\rangle_{\text{as}} = \frac{1}{\sqrt{6}} \mathcal{A}_{123} |123\rangle$ , so that  $\langle 1'2'3' | \mathcal{A}_{123} V_{3N} | 123 \rangle = {}_{\text{as}} \langle 1'2'3' | V_{3N} | 123 \rangle_{\text{as}}$ . Diagrammatically, Eq. (13) corresponds to connecting one incoming and one outgoing line in the antisymmetrized 3N force with a noninteracting propagator:

$$\text{Diagrammatic equation (14): } \text{Left side: } V_{3N} \text{ box with 6 lines. Right side: } V_{3N} \text{ box with 4 lines and a loop labeled } k_3 \sigma_3. \quad (14)$$

The resulting density-dependent two-body interaction  $\bar{V}_{3N}$  corresponds to the normal-ordered two-body part of 3N forces (for normal-ordering, see Refs. [26, 27]), where

the normal ordering is with respect to the Fermi sea. As a result, the antisymmetrized  $\bar{V}_{3N}$  is added to the antisymmetrized NN interaction  $V_{\text{NN,as}} = (1 - P_{12}) V_{\text{NN}}$  when evaluating two-body contributions beyond the Hartree-Fock level. For the Hartree-Fock (or normal-ordered zero-body) contribution, the 3N diagram has a symmetry factor 1/6, so that  $\bar{V}_{3N}/3$  is added to  $V_{\text{NN,as}}$  at the Hartree-Fock level (see Sect. III A). For one-body contributions, normal ordering leads to  $\bar{V}_{3N}/2$  being added to  $V_{\text{NN,as}}$ , for example, for the first-order contribution to the self-energy. These factors ensure the correct symmetry factors for diagrams involving NN and 3N interactions. The above normal-ordering factors may not always be taken into account properly in the literature [28–30] (for example, it is incorrect to use  $V_{\text{NN,as}} + \bar{V}_{3N}/3$  or  $V_{\text{NN,as}} + \bar{V}_{3N}$  for both Hartree-Fock and higher-order contributions).

In addition to the density dependence, the two-body interaction  $\bar{V}_{3N}$  depends on the incoming and outgoing relative momenta,  $\mathbf{k} = (\mathbf{k}_1 - \mathbf{k}_2)/2$  and  $\mathbf{k}' = (\mathbf{k}'_1 - \mathbf{k}'_2)/2$ , on the spin of particles 1 and 2, and on the two-body center-of-mass momentum  $\mathbf{P} = \mathbf{k}_1 + \mathbf{k}_2 = \mathbf{k}'_1 + \mathbf{k}'_2$ . However, as will be shown in Sect. III A, the  $P$  dependence is weak compared to the dependence on the relative momenta. This can be understood from the momentum transfers in the pion propagators of Fig. 1. The momentum transfers in the first two diagrams are  $\mathbf{k} - \mathbf{k}'$ , 0 (for the left and right propagators) and  $\mathbf{k} + \mathbf{k}'$ , 0. While these terms vanish in the considered case of  $V_c$ , the only weak  $P$  dependence would arise from the regulator functions in Eq. (12). For the remaining four diagrams in Fig. 1, the momentum transfers are  $\mathbf{k} \pm \mathbf{k}'$ ,  $\mathbf{P}/2 \pm \mathbf{k}' - \mathbf{k}_3$  and  $\mathbf{P}/2 + \mathbf{k} - \mathbf{k}_3$ ,  $\mathbf{P}/2 \pm \mathbf{k}' - \mathbf{k}_3$ . Therefore, the  $P$  dependence is only through  $\mathbf{k}'_3 = \mathbf{P}/2 - \mathbf{k}_3$  and can be transformed into a dependence due to  $n_{\mathbf{P}/2 - \mathbf{k}'_3}$  (by substitution in the integral) and through the regulator functions. For typical center-of-mass momenta  $P \lesssim k_F$ , this results in the weak  $P$  dependence.

For the derivation of  $\bar{V}_{3N}$ , we use Mathematica and automate the momentum and spin exchange operations by representing all spin operators in matrix form. The antisymmetrized 3N force in neutron matter, Eq. (12), is represented in this explicit three-particle spin basis and for general particle momenta  $\mathbf{k}_i$ . We then perform the spin trace over the third particle and project the resulting two-body matrix on a complete set of two-body spin operators. In this way, we obtain a general operator structure of  $\bar{V}_{3N}$  in spin-saturated neutron matter in terms of a set of basic integral functions. Only at this point we

transform  $\bar{V}_{3N}$  to the relative and center-of-mass basis and adapt a fixed- $P$  approximation. Since the number of spin operators is minimal for  $P = 0$ , we take  $P = 0$  for simplicity and our final result is given by

$$\bar{V}_{3N} = \frac{g_A^2}{4f_\pi^4} \left[ -2c_1 m_\pi^2 A_{12}(\mathbf{k}, \mathbf{k}') + c_3 B_{12}(\mathbf{k}, \mathbf{k}') \right], \quad (15)$$

where the functions  $A_{12}(\mathbf{k}, \mathbf{k}')$  and  $B_{12}(\mathbf{k}, \mathbf{k}')$  include all spin dependences,

$$\begin{aligned} A_{12}(\mathbf{k}, \mathbf{k}') &= 2 \left[ \rho_+^2(\mathbf{k}, \mathbf{k}') + 2a^1(\mathbf{k}, \mathbf{k}') - a^1(\mathbf{k}, -\mathbf{k}') - \bar{b}^1(\mathbf{k}, \mathbf{k}') \right] \\ &\quad - \frac{2}{3} \boldsymbol{\sigma}_1 \cdot \boldsymbol{\sigma}_2 \left[ 2\rho_-^2(\mathbf{k}, \mathbf{k}') + \rho_+^2(\mathbf{k}, \mathbf{k}') + 3a^1(\mathbf{k}, -\mathbf{k}') - \bar{b}^1(\mathbf{k}, \mathbf{k}') - 2\bar{b}^1(\mathbf{k}, -\mathbf{k}') \right] \\ &\quad + 4 \left[ S_{12}(\mathbf{k} + \mathbf{k}') \rho_+^0(\mathbf{k}, \mathbf{k}') - S_{12}(\mathbf{k} - \mathbf{k}') \rho_-^0(\mathbf{k}, \mathbf{k}') \right] - 4 \boldsymbol{\sigma}_1^a \boldsymbol{\sigma}_2^b \left[ \bar{d}_{ab}^0(\mathbf{k}, \mathbf{k}') - \bar{d}_{ab}^0(\mathbf{k}, -\mathbf{k}') \right] \\ &\quad - 2i (\boldsymbol{\sigma}_1 + \boldsymbol{\sigma}_2)^a \left[ c_a^0(\mathbf{k}, \mathbf{k}') - c_a^0(\mathbf{k}, -\mathbf{k}') \right], \end{aligned} \quad (16)$$

$$\begin{aligned} B_{12}(\mathbf{k}, \mathbf{k}') &= -2 \left[ \rho_+^4(\mathbf{k}, \mathbf{k}') + 2a^2(\mathbf{k}, \mathbf{k}') - a^2(\mathbf{k}, -\mathbf{k}') - \bar{b}^2(\mathbf{k}, \mathbf{k}') \right] \\ &\quad + \frac{2}{3} \boldsymbol{\sigma}_1 \cdot \boldsymbol{\sigma}_2 \left[ 2\rho_-^4(\mathbf{k}, \mathbf{k}') + \rho_+^4(\mathbf{k}, \mathbf{k}') + 3a^2(\mathbf{k}, -\mathbf{k}') - \bar{b}^2(\mathbf{k}, \mathbf{k}') - 2\bar{b}^2(\mathbf{k}, -\mathbf{k}') \right] \\ &\quad - 4 \left[ S_{12}(\mathbf{k} + \mathbf{k}') \rho_+^2(\mathbf{k}, \mathbf{k}') - S_{12}(\mathbf{k} - \mathbf{k}') \rho_-^2(\mathbf{k}, \mathbf{k}') \right] + 4 \boldsymbol{\sigma}_1^a \boldsymbol{\sigma}_2^b \left[ \bar{d}_{ab}^1(\mathbf{k}, \mathbf{k}') - \bar{d}_{ab}^1(\mathbf{k}, -\mathbf{k}') \right] \\ &\quad + 2i (\boldsymbol{\sigma}_1 + \boldsymbol{\sigma}_2)^a \left[ c_a^1(\mathbf{k}, \mathbf{k}') - c_a^1(\mathbf{k}, -\mathbf{k}') \right], \end{aligned} \quad (17)$$

and the basic integral functions are defined by

$$\rho_\pm^n(\mathbf{k}, \mathbf{k}') = \frac{(\mathbf{k} \pm \mathbf{k}')^n}{((\mathbf{k} \pm \mathbf{k}')^2 + m_\pi^2)^2} \int_{\mathbf{k}_3} 1, \quad (18)$$

$$a^n(\mathbf{k}, \mathbf{k}') = \int_{\mathbf{k}_3} \frac{((\mathbf{k} + \mathbf{k}_3) \cdot (\mathbf{k}' + \mathbf{k}_3))^n}{((\mathbf{k} + \mathbf{k}_3)^2 + m_\pi^2)((\mathbf{k}' + \mathbf{k}_3)^2 + m_\pi^2)}, \quad (19)$$

$$b^n(\mathbf{k}, \mathbf{k}') = \int_{\mathbf{k}_3} \frac{((\mathbf{k} + \mathbf{k}') \cdot (\mathbf{k} + \mathbf{k}_3))^n}{((\mathbf{k} + \mathbf{k}')^2 + m_\pi^2)((\mathbf{k} + \mathbf{k}_3)^2 + m_\pi^2)}, \quad (20)$$

$$c_a^n(\mathbf{k}, \mathbf{k}') = \int_{\mathbf{k}_3} \frac{((\mathbf{k} + \mathbf{k}_3) \cdot (\mathbf{k}' + \mathbf{k}_3))^n ((\mathbf{k} + \mathbf{k}_3) \times (\mathbf{k}' + \mathbf{k}_3))_a}{((\mathbf{k} + \mathbf{k}_3)^2 + m_\pi^2)((\mathbf{k}' + \mathbf{k}_3)^2 + m_\pi^2)}, \quad (21)$$

$$d_{ab}^n(\mathbf{k}, \mathbf{k}') = \int_{\mathbf{k}_3} ((\mathbf{k} + \mathbf{k}') \cdot (\mathbf{k} + \mathbf{k}_3))^n \frac{(\mathbf{k} + \mathbf{k}')_a (\mathbf{k} + \mathbf{k}_3)_b + (\mathbf{k} + \mathbf{k}')_b (\mathbf{k} + \mathbf{k}_3)_a - \frac{2}{3} \delta_{ab} (\mathbf{k} + \mathbf{k}') \cdot (\mathbf{k} + \mathbf{k}_3)}{2((\mathbf{k} + \mathbf{k}')^2 + m_\pi^2)((\mathbf{k} + \mathbf{k}_3)^2 + m_\pi^2)}. \quad (22)$$

In Eqs. (16)–(22), the indices  $a, b$  run over the three components of the spin operators, the tensor operator is given by  $S_{12}(\mathbf{p}) = (\boldsymbol{\sigma}_1 \cdot \mathbf{p})(\boldsymbol{\sigma}_2 \cdot \mathbf{p}) - p^2 \boldsymbol{\sigma}_1 \cdot \boldsymbol{\sigma}_2 / 3$ , and the overline denotes a symmetrization in the relative momentum variables,  $\bar{x}(\mathbf{k}, \mathbf{k}') = x(\mathbf{k}, \mathbf{k}') + x(\mathbf{k}', \mathbf{k})$ . In addition, we have introduced the short-hand notation for the integration over the momentum of the third particle,

$$\int_{\mathbf{k}_3} = \int \frac{d\mathbf{k}_3}{(2\pi)^3} n_{\mathbf{k}_3} \tilde{f}_R(k', k_3) \tilde{f}_R(k, k_3), \quad (23)$$

where the regulator, Eq. (7), expressed in terms of the

relative and third-particle momenta for  $P = 0$  is given by  $\tilde{f}_R(k, k_3) = \exp[-(k^2 + k_3^2/3)^2 / \Lambda_{3NF}^4]$ .

The density-dependent two-body interaction  $\bar{V}_{3N}$  includes all spin structures that are invariant under combined rotations in spin and space in a spin-saturated system. In addition to the central spin-independent and spin-spin ( $\boldsymbol{\sigma}_1 \cdot \boldsymbol{\sigma}_2$ ) interactions, the functions  $A_{12}$  and  $B_{12}$  include tensor forces ( $S_{12}$ ), spin-orbit interactions ( $c_a^n$ -terms) and additional tensor structures ( $d_{ab}^n$ -terms), which can be expressed in terms of  $S_{12}$  and quadratic spin-orbit interactions. Finally, we have checked that

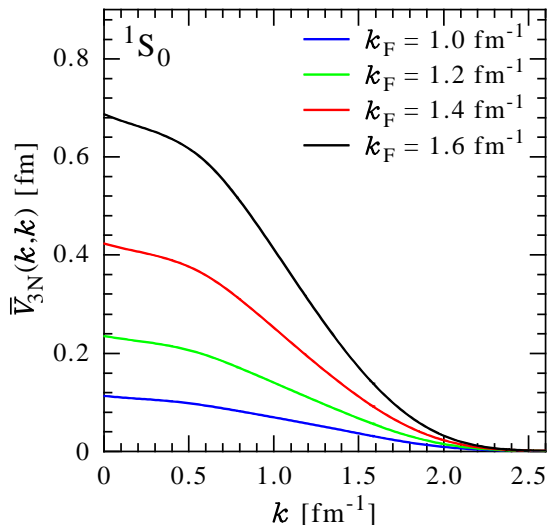


FIG. 2: (Color online) Diagonal momentum-space matrix elements of the density-dependent two-body interaction  $\bar{V}_{3N}$  for  $P = 0$  in the  $^1S_0$  channel. Results with  $\Lambda_{3NF} = 2.0 \text{ fm}^{-1}$  are shown versus relative momentum  $k$  for different Fermi momenta  $k_F = 1.0, 1.2, 1.4$  and  $1.6 \text{ fm}^{-1}$  (increasing in strength) in neutron matter.

$\bar{V}_{3N}$  is even (odd) in the scattering angle  $\theta_{\mathbf{k}, \mathbf{k}'}$  in the two-body spin  $S = 0$  ( $S = 1$ ) channel.

### C. Partial-wave matrix elements of $\bar{V}_{3N}$

Next, we expand  $\bar{V}_{3N}$  in two-body partial waves and show the diagonal momentum-space matrix elements in Figs. 2 and 3 in the  $^1S_0$  and the spin-triplet  $P$ -wave channels for different Fermi momenta  $k_F = 1.0, 1.2, 1.4$  and  $1.6 \text{ fm}^{-1}$  (in units where  $\hbar^2/m = 1$ , with nucleon mass  $m$ ). The partial-wave matrix elements are normalized to the direct term (as for NN interactions). In Figs. 2 and 3, we have interpolated between the momentum mesh points. To set the scale, a typical  $S$ -wave strength for low-momentum NN interactions is  $V_{\text{low } k}(0, 0) \sim -2.0 \text{ fm}$  [11, 12], but the relative 3N strength depends on whether  $\bar{V}_{3N}$  is used at the Hartree-Fock, one- or two-body level (see Sects. III A to III C). We find that the dominant partial wave is the  $^1S_0$  channel, which is found to be repulsive. In addition, for  $k_F = 1.6 \text{ fm}^{-1}$  we plot in Fig. 3 the central and central plus tensor parts of  $\bar{V}_{3N}$ . Because  $S_{12}(\mathbf{p})/p^2 = -4/3, 2/3$  and  $-2/15$  in the  $^3P_0, ^3P_1$  and  $^3P_2$  channels, we conclude from Fig. 3 that the tensor force in  $\bar{V}_{3N}$  is repulsive. Moreover, with  $\mathbf{L} \cdot \mathbf{S} = -2, -1$  and  $1$  in the  $^3P_0, ^3P_1$  and  $^3P_2$  channels, we observe that the spin-orbit interaction in  $\bar{V}_{3N}$  (determined by the difference of the solid and dashed lines) is attractive.

The density dependence of the two-body matrix elements depends on the partial wave. In the  $^1S_0$  channel this dependence can be approximately parameterized

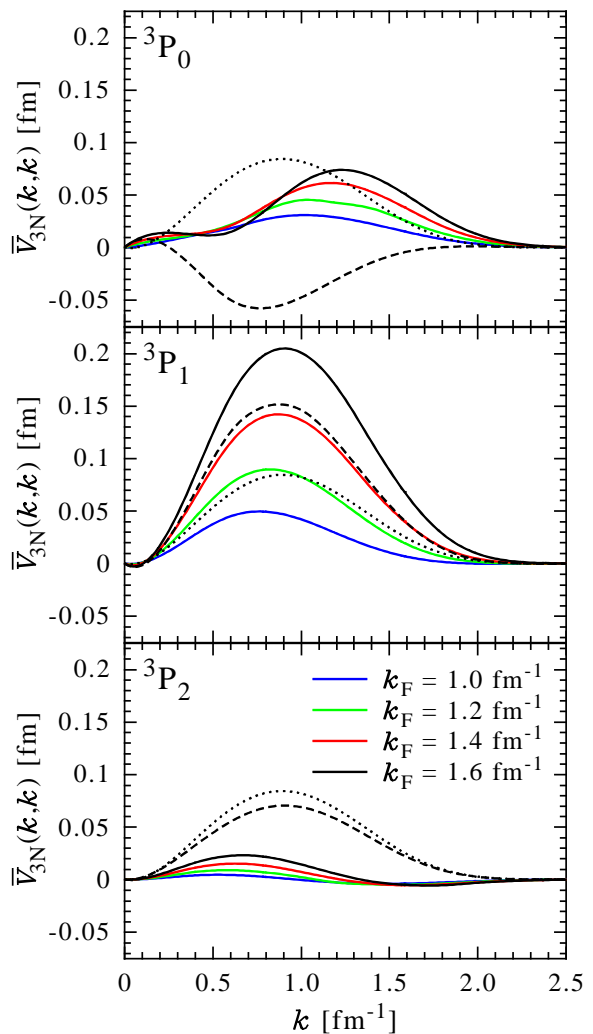


FIG. 3: (Color online) Diagonal momentum-space matrix elements of the density-dependent two-body interaction  $\bar{V}_{3N}$  for  $P = 0$  in the spin-triplet  $P$ -wave channels. Results with  $\Lambda_{3NF} = 2.0 \text{ fm}^{-1}$  are shown versus relative momentum  $k$  for different Fermi momenta  $k_F = 1.0, 1.2, 1.4$  and  $1.6 \text{ fm}^{-1}$  (increasing in strength). For  $k_F = 1.6 \text{ fm}^{-1}$ , the dotted lines represent the central parts (degenerate in  $J$ ) of  $\bar{V}_{3N}$ , whereas the dashed lines include the central plus tensor interactions (without the  $c_a''$ -terms in Eqs. (16) and (17)).

by a power of the Fermi momentum,  $\bar{V}_{3N}(k', k, k_F) \approx F(k', k) (k_F/\bar{k}_F)^4$ , with some reference Fermi momentum  $\bar{k}_F$ . In the spin-triplet channels this is more complex due to the different momentum and density dependences of the various operator structures in  $\bar{V}_{3N}$ .

Finally, it is possible to improve the  $P = 0$  approximation and to perform the sum over the third particle self-consistently, which corresponds to closing the line in Eq. (14) with the self-consistent propagator. For finite  $P$ , one has more allowed spin operators with more complex integral functions that can depend on  $P$  but also on the angle of  $\mathbf{P}$  with respect to  $\mathbf{k}$  and  $\mathbf{k}'$ . Since  $\bar{V}_{3N}$  has been

derived using Mathematica for general particle momenta  $\mathbf{k}_i$ , this is directly possible. One could then explore angle-averaging over  $\hat{\mathbf{P}}$  or averaging over the magnitude of  $\mathbf{P}$ . However, as will be shown in the next section, the  $P = 0$  approximation is reliable for bulk properties and neutron matter based on chiral low-momentum interactions is sufficiently perturbative, which justifies using the non-interacting density to sum over the third particle.

### III. RESULTS

We apply the developed density-dependent two-body interaction  $\bar{V}_{3N}$  to calculate the properties of neutron matter in a loop expansion around the Hartree-Fock energy. These are the first results for neutron matter based on chiral EFT interactions and including N<sup>2</sup>LO 3N forces. The many-body calculation follows the strategy of Refs. [7, 8, 25], but with significant improvements for the second-order contributions involving  $\bar{V}_{3N}$  and with fully self-consistent single-particle energies.

#### A. Hartree-Fock and $P$ dependence of $\bar{V}_{3N}$

The contributions to the Hartree-Fock energy are shown diagrammatically in Fig. 4 and the first-order NN and 3N interaction energies are given by

$$\frac{E_{\text{NN}}^{(1)}}{V} = \frac{1}{2} \text{Tr}_{\sigma_1} \text{Tr}_{\sigma_2} \int \frac{d\mathbf{k}_1}{(2\pi)^3} \int \frac{d\mathbf{k}_2}{(2\pi)^3} \times n_{\mathbf{k}_1} n_{\mathbf{k}_2} \langle 12 | (1 - P_{12}) V_{\text{low } k} |_{nn} | 12 \rangle, \quad (24)$$

$$\frac{E_{3N}^{(1)}}{V} = \frac{1}{6} \text{Tr}_{\sigma_1} \text{Tr}_{\sigma_2} \text{Tr}_{\sigma_3} \int \frac{d\mathbf{k}_1}{(2\pi)^3} \int \frac{d\mathbf{k}_2}{(2\pi)^3} \int \frac{d\mathbf{k}_3}{(2\pi)^3} \times n_{\mathbf{k}_1} n_{\mathbf{k}_2} n_{\mathbf{k}_3} f_{\text{R}}^2(p, q) \langle 123 | \mathcal{A}_{123} V_{3N} |_{nnn} | 123 \rangle, \quad (25)$$

where  $V$  is the volume and we use the shorthand notation  $i \equiv \mathbf{k}_i \sigma_i$  in the bra and ket states. The momentum-conserving delta functions are not included in the NN and 3N matrix elements. It is evident from Eq. (25) that the correct 3N symmetry factor is obtained when the antisymmetrized two-body interaction  $V_{\text{as}}^{(0)} = (1 - P_{12}) V_{\text{low } k} + \bar{V}_{3N}/3$  is used at the Hartree-Fock level. With the expansion in two-body partial waves, we have

$$\frac{E_{\text{NN}}^{(1)} + E_{3N}^{(1)}}{V} = \frac{1}{\pi^3} \int k^2 dk \int P^2 dP \int d\cos\theta_{\mathbf{k}, \mathbf{P}} \times n_{\frac{\mathbf{P}}{2} + \mathbf{k}} n_{\frac{\mathbf{P}}{2} - \mathbf{k}} \sum_{S, l, J} (2J+1) \langle k | V_{SllJ}^{(0)} | k \rangle (1 - (-1)^{l+S+1}). \quad (26)$$

In Eq. (26) and in the following, all partial-wave matrix elements are normalized to the direct term, so that

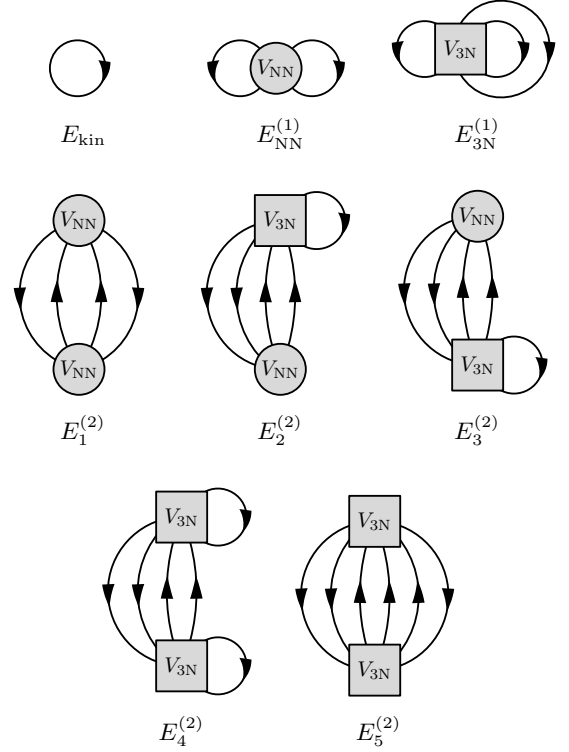


FIG. 4: Top row: Diagrams contributing to the Hartree-Fock energy. These include the kinetic energy  $E_{\text{kin}}$  and the first-order NN and 3N interaction energies,  $E_{\text{NN}}^{(1)}$  and  $E_{3N}^{(1)}$ . Middle and bottom rows: Second-order contributions to the energy due to NN-NN interactions  $E_1^{(2)}$ , NN-3N and 3N-3N interactions, where 3N forces enter as density-dependent two-body interactions,  $E_{2,3}^{(2)}$  and  $E_4^{(2)}$ , respectively, and the remaining 3N-3N diagram  $E_5^{(2)}$ .

$$V_{SllJ}^{(0)} = V_{\text{low } k, SllJ} + \bar{V}_{3N, SllJ}/6.$$

For N<sup>2</sup>LO 3N forces, the first-order 3N interaction energy has been calculated exactly in Ref. [25], without the fixed- $P$  approximation in  $\bar{V}_{3N}$ ,

$$\frac{E_{3N}^{(1)}}{V} = \frac{g_A^2}{f_\pi^4} \int \frac{d\mathbf{k}_1 d\mathbf{k}_2 d\mathbf{k}_3}{(2\pi)^9} n_{\mathbf{k}_1} n_{\mathbf{k}_2} n_{\mathbf{k}_3} f_{\text{R}}^2(p, q) \times \left[ -2c_1 m_\pi^2 \left( \frac{\mathbf{k}_{12} \cdot \mathbf{k}_{23}}{(k_{12}^2 + m_\pi^2)(k_{23}^2 + m_\pi^2)} + \frac{k_{12}^2}{(k_{12}^2 + m_\pi^2)^2} \right) + c_3 \left( \frac{(\mathbf{k}_{12} \cdot \mathbf{k}_{23})^2}{(k_{12}^2 + m_\pi^2)(k_{23}^2 + m_\pi^2)} - \frac{k_{12}^4}{(k_{12}^2 + m_\pi^2)^2} \right) \right], \quad (27)$$

with  $\mathbf{k}_{ij} = \mathbf{k}_i - \mathbf{k}_j$ . By comparing the Hartree-Fock energy with the density-dependent two-body interaction  $\bar{V}_{3N}$  for  $P = 0$ , Eq. (26), to the result with the full first-order 3N energy, Eq. (27), we can assess the reliability of the  $P = 0$  approximation in  $\bar{V}_{3N}$ . Our results for  $E_{\text{NN}+3N, \text{eff}}^{(1)} = E_{\text{kin}} + E_{\text{NN}}^{(1)} + E_{3N}^{(1)}$  in comparison to the full Hartree-Fock energy  $E_{\text{NN}+3N, \text{full}}^{(1)}$  are shown for densities  $\rho < 0.16 \text{ fm}^{-3}$  (below saturation density

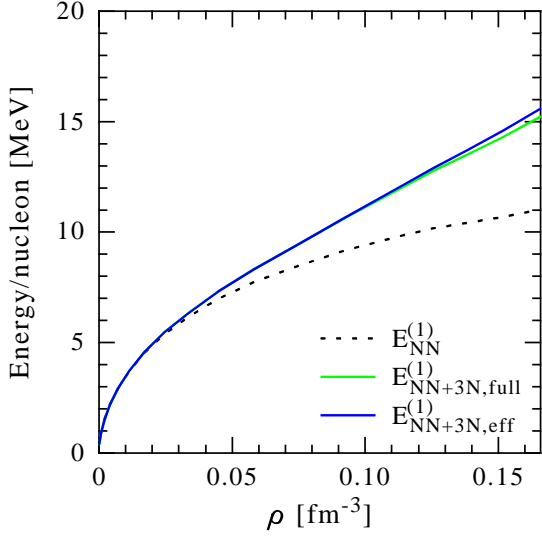


FIG. 5: (Color online) Energy per particle  $E/N$  of neutron matter as a function of density  $\rho$  at the Hartree-Fock level, based on low-momentum chiral NN and 3N interactions with  $\Lambda/\Lambda_{3NF} = 2.0 \text{ fm}^{-1}$ . The first-order energy  $E_{3N,\text{eff}}^{(1)}$  using  $\bar{V}_{3N}$  with  $P = 0$  is compared to the exact Hartree-Fock energy  $E_{3N,\text{full}}^{(1)}$ . To show the impact of chiral 3N forces, we also give the first-order energy based only on NN interactions.

$\rho_0 = 0.16 \text{ fm}^{-3}$ ) in Fig. 5. The  $P = 0$  approximation for  $\bar{V}_{3N}$  leads to energies that agree very well with the exact result at the Hartree-Fock level. For saturation density ( $k_F = 1.7 \text{ fm}^{-1}$ ), the difference is 340 keV, while for lower  $k_F$ , the differences are always below 100 keV, as documented in Table I. This is very encouraging for evaluating higher-order contributions, where calculations with full 3N forces become increasingly more complex than with two-body interactions.

As expected from the partial-wave matrix elements, we

find in Fig. 5 that chiral 3N forces at first order increase the neutron matter energy with increasing density, compared to results based only on low-momentum NN interactions. This repulsion is due to the central parts of  $\bar{V}_{3N}$ , because noncentral forces do not contribute to the Hartree-Fock energy.

## B. Second order: single-particle energies

For the contributions beyond Hartree-Fock, we need to calculate the single-particle energies  $\varepsilon_{\mathbf{k}}$ . These are determined by the self-consistent solution to the Dyson equation. To second order, we have

$$\varepsilon_{\mathbf{k}} = \frac{k^2}{2m} + \Sigma^{(1)}(k) + \text{Re} \Sigma^{(2)}(k, \varepsilon_{\mathbf{k}}). \quad (28)$$

Here  $\Sigma^{(1)}$  denotes the first-order NN and 3N contributions to the self-energy, which are real,  $\Sigma^{(2)}$  includes the second-order two-particle-one-hole and two-hole-one-particle terms, and the self-energy is averaged over the single-particle spin. The diagrams contributing to the self-energy to second order are given by

$$\Sigma = V + V \quad (29)$$

The resulting first- and second-order self-energies can be expressed in terms of two-body partial waves and one has (see also Ref. [31])

$$\Sigma^{(1)}(k_1) = \frac{1}{2\pi} \int k_2^2 dk_2 \int d \cos \theta_{\mathbf{k}_1, \mathbf{k}_2} n_{\mathbf{k}_2} \sum_{S,l,J} (2J+1) \langle k_{12}/2 | V_{SUJ}^{(1)} | k_{12}/2 \rangle (1 - (-1)^{l+S+1}), \quad (30)$$

$$\begin{aligned} \Sigma^{(2)}(k_1, \omega_1) &= \frac{4}{k_1 \pi^2} \int P dP \int k dk \int d\mathbf{k}' \sum_{S, M_S, M'_S} \sum_{l, l', m, m', m''} \sum_{J, M} i^{l'-l''} Y_{lm}^*(\hat{\mathbf{k}}) Y_{lm}(\hat{\mathbf{k}}) Y_{l'm'}(\hat{\mathbf{k}}') Y_{l''m''}^*(\hat{\mathbf{k}}') \\ &\times (\mathcal{C}_{lmSM_S}^{JM})^2 \mathcal{C}_{l'm'SM'_S}^{JM} \mathcal{C}_{l''m''SM''_S}^{JM} \langle k | V_{SUJ}^{(2)} | k' \rangle \langle k' | V_{SUJ}^{(2)} | k \rangle (1 - (-1)^{l+S+1}) (1 - (-1)^{l'+S+1}) \\ &\times \left[ \frac{(1 - n_{\frac{\mathbf{P}}{2} + \mathbf{k}'})(1 - n_{\frac{\mathbf{P}}{2} - \mathbf{k}'}) n_{\mathbf{P} - \mathbf{k}_1}}{\omega_1 + \varepsilon_{\mathbf{P} - \mathbf{k}_1} - \varepsilon_{\frac{\mathbf{P}}{2} + \mathbf{k}'} - \varepsilon_{\frac{\mathbf{P}}{2} - \mathbf{k}'} + i\delta} + \frac{n_{\frac{\mathbf{P}}{2} + \mathbf{k}'} n_{\frac{\mathbf{P}}{2} - \mathbf{k}'} (1 - n_{\mathbf{P} - \mathbf{k}_1})}{\omega_1 + \varepsilon_{\mathbf{P} - \mathbf{k}_1} - \varepsilon_{\frac{\mathbf{P}}{2} + \mathbf{k}'} - \varepsilon_{\frac{\mathbf{P}}{2} - \mathbf{k}'} - i\delta} \right], \end{aligned} \quad (31)$$

where  $\mathcal{C}_{lmSM_S}^{JM}$  denote Clebsch-Gordan coefficients and  $Y_{lm}(\hat{\mathbf{k}})$  are spherical harmonics. In Eq. (31), the  $z$ -

axis is taken in the  $\mathbf{P}$  direction, we have used  $k dk = P k_1 d\hat{\mathbf{k}}_1 / (4\pi)$ , and  $\mathbf{k} = \mathbf{k}_1 - \mathbf{P}/2$  determines the ar-

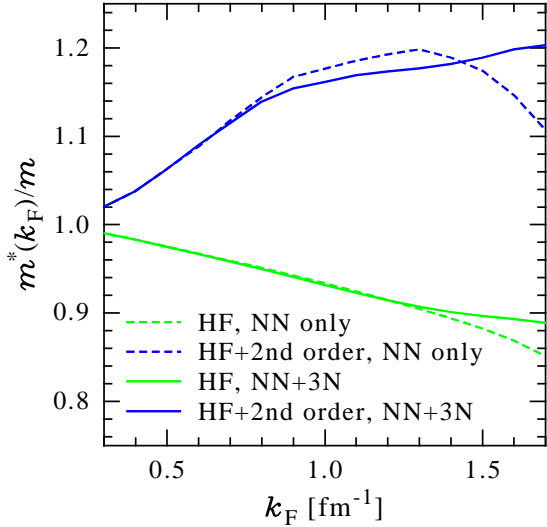


FIG. 6: (Color online) Effective mass  $m^*(k_F)/m$  at the Fermi surface as a function of Fermi momentum  $k_F$  in neutron matter. Results for  $\Lambda/\Lambda_{3\text{NF}} = 2.0 \text{ fm}^{-1}$  are shown at the Hartree-Fock level, plus second-order contributions, and based only on NN interactions for comparison. At second order, the effective mass includes  $k$ -mass and  $e$ -mass effects.

gument  $\hat{\mathbf{k}}$ . As discussed in Sect. II B, the antisymmetrized two-body interactions in the first- and second-order terms are given by  $V_{\text{as}}^{(1)} = (1 - P_{12})V_{\text{low } k} + \bar{V}_{3\text{N}}/2$  and  $V_{\text{as}}^{(2)} = (1 - P_{12})V_{\text{low } k} + \bar{V}_{3\text{N}}$ , with partial waves  $V_{S\tilde{L}J}^{(1)} = V_{\text{low } k, S\tilde{L}J} + \bar{V}_{3\text{N}, S\tilde{L}J}/4$  and  $V_{S\tilde{L}J}^{(2)} = V_{\text{low } k, S\tilde{L}J} + \bar{V}_{3\text{N}, S\tilde{L}J}/2$ .

We solve the Dyson equation, Eq. (28), self-consistently using the self-energies given by Eqs. (30) and (31). In Fig. 6, we show the resulting effective mass at the Fermi surface,

$$\frac{m^*(k_F)}{m} = \left( \frac{m}{k} \frac{d\varepsilon_{\mathbf{k}}}{dk} \right)^{-1} \Big|_{k=k_F}. \quad (32)$$

At the Hartree-Fock level, 3N contributions only change the effective mass marginally. Including second-order contributions leads to the typical enhancement of the effective mass at the Fermi surface, and we find a larger impact of 3N forces for  $k_F > 1.3 \text{ fm}^{-1}$ .

### C. Second order: energy per particle

We include the second-order contributions  $E_1^{(2)}$  to  $E_4^{(2)}$  of Fig. 4, which are given by

$$E_{\text{NN}+3\text{N}, \text{eff}}^{(2)} = \frac{1}{4} \left( \prod_{i=1}^4 \text{Tr}_{\sigma_i} \int \frac{d\mathbf{k}_i}{(2\pi)^3} \right) |\langle 12 | V_{\text{as}}^{(2)} | 34 \rangle|^2 \times \frac{n_{\mathbf{k}_1} n_{\mathbf{k}_2} (1 - n_{\mathbf{k}_3}) (1 - n_{\mathbf{k}_4})}{\varepsilon_{\mathbf{k}_1} + \varepsilon_{\mathbf{k}_2} - \varepsilon_{\mathbf{k}_3} - \varepsilon_{\mathbf{k}_4}} (2\pi)^3 \delta(\mathbf{k}_1 + \mathbf{k}_2 - \mathbf{k}_3 - \mathbf{k}_4). \quad (33)$$

As in the second-order self-energy, the antisymmetrized two-body interactions when evaluating contributions beyond the Hartree-Fock level are given by  $V_{\text{as}}^{(2)} = (1 - P_{12})V_{\text{low } k} + \bar{V}_{3\text{N}}$ . The second-order calculations are carried out using the self-consistent single-particle energies determined by solving the Dyson equation, Eq. (28), as discussed in Sect. III B, and the intermediate-state phase-space integrations are performed fully. Summing over the spins and expanding in partial waves, we have [25]

$$\begin{aligned} & \sum_{S, M_S, M'_S} |\langle \mathbf{k} S M_S | V_{\text{as}}^{(2)} | \mathbf{k}' S M'_S \rangle|^2 = \sum_L P_L(\cos \theta_{\mathbf{k}, \mathbf{k}'}) \\ & \times \sum_{J, l, l', S} \sum_{\tilde{J}, \tilde{l}, \tilde{l}'} (4\pi)^2 i^{(l-l'+\tilde{l}-\tilde{l}')} (-1)^{\tilde{l}+l'+L} C_{l0\tilde{l}0}^{L0} C_{l'0\tilde{l}'0}^{L0} \\ & \times \sqrt{(2l+1)(2l'+1)(2\tilde{l}+1)(2\tilde{l}'+1)(2J+1)(2\tilde{J}+1)} \\ & \times \left\{ \begin{matrix} l & S & J \\ \tilde{J} & L & \tilde{l}' \end{matrix} \right\} \left\{ \begin{matrix} J & S & l' \\ \tilde{l} & L & \tilde{J} \end{matrix} \right\} \langle k | V_{S\tilde{l}'J}^{(2)} | k' \rangle \langle k' | V_{S\tilde{l}J}^{(2)} | k \rangle \\ & \times (1 - (-1)^{l+S+1}) (1 - (-1)^{\tilde{l}+S+1}), \end{aligned} \quad (34)$$

where  $\{\dots\}$  denote 6j-symbols and  $P_L(\cos \theta)$  are Legendre polynomials. Keeping only  $L = 0$  in Eq. (34) corresponds to the angle-averaging approximation for the Pauli-blocking operator, but we keep all  $L \leq 6$  for  $V_{\text{low } k}$  and  $L \leq 4$  for  $\bar{V}_{3\text{N}}$ .

Our second-order results for the neutron matter energy,  $E_{\text{NN}+3\text{N}, \text{eff}} = E_{\text{NN}+3\text{N}, \text{eff}}^{(1)} + E_{\text{NN}+3\text{N}, \text{eff}}^{(2)}$ , are presented in Fig. 7. The different contributions are listed in Table I. We observe that the cutoff dependence is reduced when going from first to second order. This is as expected based on the nuclear matter results [7, 8], but for neutron matter the cutoff dependence is significantly weaker already at the Hartree-Fock level. The cutoff dependence increases with density and is less than 1 MeV per particle for the densities studied in Fig. 7 over the cutoff range  $1.8 \text{ fm}^{-1} \leq \Lambda \leq 2.8 \text{ fm}^{-1}$  and  $2.0 \text{ fm}^{-1} \leq \Lambda_{3\text{NF}} \leq 2.5 \text{ fm}^{-1}$ . This band sets the scale for omitted short-range many-body contributions and we discuss the theoretical uncertainties in the long-range parts in the following section. The weak cutoff dependence also demonstrates that the average momentum in the system (which is smaller than the Fermi momentum, because  $\langle p_i^2 \rangle = 3/5 k_F^2$ ) is well below the cutoff.

Moreover, we have found that self-energy corrections to the neutron matter energy are practically negligible. The second-order energy with  $\Sigma = 0$  is within 200 keV of the self-consistent results shown in Fig. 7. In addition, the second-order energy contributions are always below 1.3 MeV per particle in Table I, except for the large cutoff  $\Lambda = 2.8 \text{ fm}^{-1}$  cases. The second-order contributions practically only improve the cutoff independence of the results without changing the energy significantly. Moreover, for the lower cutoffs, the Hartree-Fock energies are already reliable. These findings combined suggest that neutron matter is perturbative at nuclear

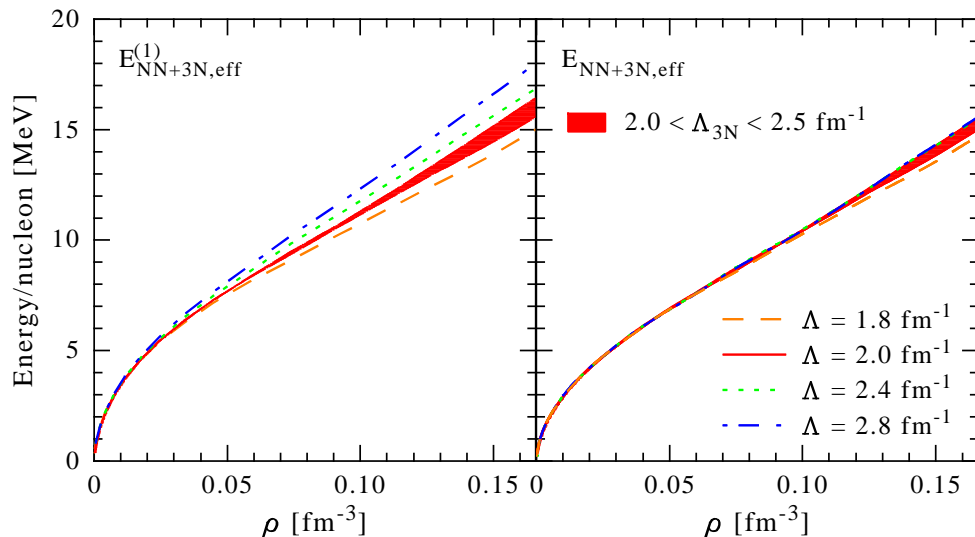


FIG. 7: (Color online) Energy per particle  $E/N$  of neutron matter as a function of density  $\rho$  at the Hartree-Fock level (left) and including second-order contributions (right). The results are based on evolved  $N^3\text{LO}$  NN potentials and  $N^2\text{LO}$  3N forces. Theoretical uncertainties are estimated by varying the NN cutoff (lines) and the 3N cutoff (band for fixed  $\Lambda = 2.0 \text{ fm}^{-1}$ ).

$k_F$	$\Lambda/\Lambda_{3\text{NF}}$	$E_{\text{kin}}$	$E_{\text{NN}}^{(1)}$	$E_{3\text{N,full}}^{(1)}$	$E_{3\text{N,eff}}^{(1)}$	$E_1^{(2)}$	$E_2^{(2)} + E_3^{(2)}$	$E_4^{(2)}$
1.3	1.8/2.0	21.01	-12.86	0.95	0.94	-0.59	0.01	-0.02
1.3	2.0/2.0	21.01	-12.58	0.95	0.94	-0.78	0.00	-0.02
1.3	2.0/2.5	21.01	-12.58	1.05	1.00	-0.77	-0.01	-0.05
1.3	2.4/2.0	21.01	-12.11	0.95	0.94	-1.10	-0.02	-0.02
1.3	2.8/2.0	21.01	-11.75	0.95	0.94	-1.46	-0.03	-0.02
1.5	1.8/2.0	27.97	-18.62	2.18	2.24	-0.39	0.01	-0.05
1.5	2.0/2.0	27.97	-18.14	2.18	2.24	-0.64	-0.01	-0.05
1.5	2.0/2.5	27.97	-18.14	2.56	2.51	-0.63	-0.04	-0.14
1.5	2.4/2.0	27.97	-17.44	2.18	2.24	-1.16	-0.05	-0.05
1.5	2.8/2.0	27.97	-16.77	2.18	2.24	-1.78	-0.08	-0.05
1.7	1.8/2.0	35.93	-25.50	4.20	4.54	-0.22	0.01	-0.07
1.7	2.0/2.0	35.93	-24.93	4.20	4.54	-0.45	-0.02	-0.08
1.7	2.0/2.5	35.93	-24.93	5.36	5.40	-0.46	-0.06	-0.31
1.7	2.4/2.0	35.93	-23.64	4.20	4.54	-1.11	-0.07	-0.08
1.7	2.8/2.0	35.93	-22.51	4.20	4.54	-2.08	-0.12	-0.09

TABLE I: Contributions to the neutron matter energy due to the diagrams of Fig. 4. Results are given for Fermi momenta  $k_F = 1.3, 1.5$  and  $1.7 \text{ fm}^{-1}$  and for different  $\Lambda/\Lambda_{3\text{NF}}$  combinations. All energies are in MeV and  $k_F, \Lambda/\Lambda_{3\text{NF}}$  are in  $\text{fm}^{-1}$ .

densities. Therefore, we are confident that the  $P = 0$  approximation for  $\bar{V}_{3\text{N}}$  is reliable, when evaluating the small second-order contributions, and that it is reasonable to neglect the residual 3N-3N diagram,  $E_5^{(2)}$ .

#### D. Sensitivity to $c_i$ uncertainties

Next, we study the sensitivity of the second-order energy to uncertainties in the  $c_i$  coefficients that determine the long-range part of  $N^2\text{LO}$  3N forces. This provides an update for chiral potentials of the results of Ref. [25]. The

$c_i$  coefficients relate  $\pi\text{N}$ , NN and 3N interactions, and the determination from  $\pi\text{N}$  scattering is, within errors, consistent with the extraction from NN waves. Present constraints for  $c_1$  and  $c_3$  are  $c_1 = -0.9_{-0.5}^{+0.2} \text{ GeV}^{-1}$  and  $c_3 = -4.7_{-1.0}^{+1.5} \text{ GeV}^{-1}$  [32]. We note that at  $N^3\text{LO}$  there are contributions that shift the  $c_i$  [10], and may lead to  $c_3$  coefficients that are smaller in magnitude. In this study, we vary  $c_i$  only in 3N forces, because of lack of  $N^3\text{LO}$  NN potentials that explore these  $c_i$  variations. However, based on the universality of  $V_{\text{low } k}$  [8, 12] (starting from chiral potentials with two different  $c_i$  sets [15, 16]), we do not expect large differences from varying  $c_1$  and  $c_3$

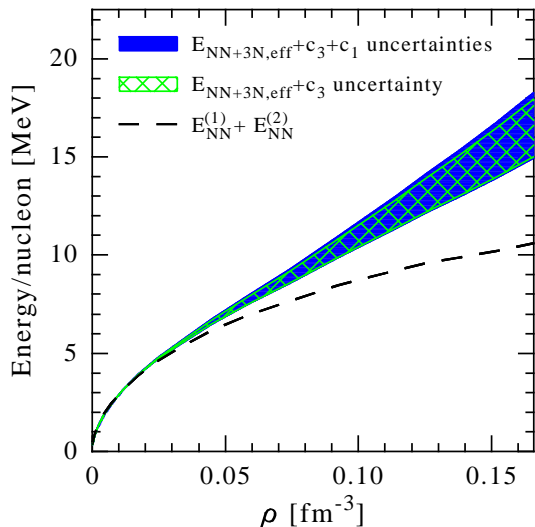


FIG. 8: (Color online) Theoretical uncertainties of the second-order energy with  $\Lambda/\Lambda_{3\text{NF}} = 2.0 \text{ fm}^{-1}$  as a function of density due to the uncertainties in the  $c_1$  and  $c_3$  coefficients of 3N forces.

in NN interactions, where these variations are also absorbed by higher-order contact interactions that have to be adjusted to reproduce NN scattering.

In Fig. 8 we show that the theoretical uncertainties of the neutron matter energy are dominated by the uncertainties in the  $c_i$  coefficients, in particular the  $c_3$  part, compared to the uncertainties of the many-body calculation or of neglected short-range many-body interactions probed by cutoff variations. The  $c_1$  and  $c_3$  variation leads to an energy uncertainty of  $\pm 1.5$  MeV per particle at saturation density. Therefore, it is important to improve the constraints on  $c_i$ . Figure 8 also shows that  $\text{N}^2\text{LO}$  3N forces provide a repulsive contribution to neutron matter at second order, even with this band.

We compare our neutron matter energy with the  $c_i$  uncertainty band to other recent neutron matter results in Fig. 9. These include Monte-Carlo calculations (GFMC  $v_6$  and  $v_8'$  [33] and QMC  $S$ -wave [2]) and di-fermion EFT results [1] for lower densities, which are only sensitive to parts of NN interactions, at very low densities only to the neutron-neutron scattering length and effective range. In addition, we include in Fig. 9 the results of Akmal *et al.* [34] based on the Argonne  $v_{18}$  NN and Urbana IX 3N potentials, where the repulsive 3N contributions arise from various terms.

### E. Symmetry energy

The spread in the energy band of Fig. 8 corresponds to a range for the symmetry energy and its density dependence. In the following we explore this correlation and consequently also a possibility of using nuclear matter properties to constrain some of the  $c_i$  couplings. As

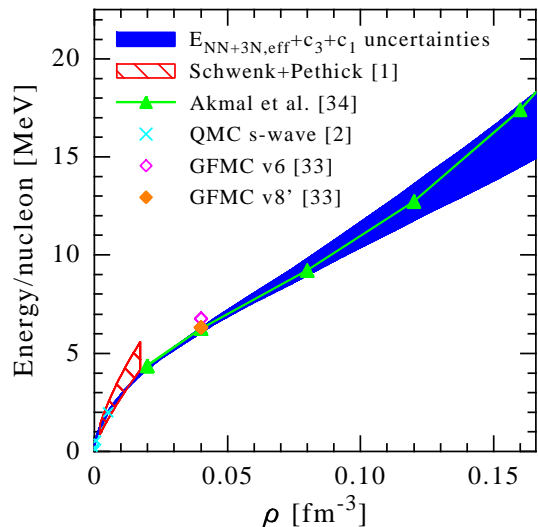


FIG. 9: (Color online) Comparison of the second-order energy with the  $c_i$  uncertainty band of Fig. 8 to other neutron matter results (see text for details).

$c_1$ [GeV]	$c_3$ [GeV]	$a_4$ [MeV]	$p_0$ [MeV $\text{fm}^{-3}$ ]
-0.81	-3.2	30.5	2.0/2.0
-0.81	-5.7	33.2	2.8/2.8
-0.7	-3.2	30.4	2.0/2.0
-1.4	-5.7	33.6	2.8/2.9

TABLE II: Symmetry energy  $a_4$  and the linear dependence of the symmetry energy  $p_0$  obtained from the energy band of Fig. 8 for different  $c_1$  and  $c_3$  coefficients using  $a_V = 16$  MeV and  $K = 190/240$  MeV.

a function of asymmetry  $\alpha = (\rho_n - \rho_p)/(\rho_n + \rho_p)$ , the energy of nuclear matter can be parameterized around saturation density as (see for example, Refs. [35, 36])

$$\frac{E(\rho, \alpha)}{A} = -a_V + \frac{K}{18\rho_0^2} (\rho - \rho_0)^2 + S_2(\rho) \alpha^2 + \dots, \quad (35)$$

with the density-dependent symmetry energy  $S_2(\rho)$ ,

$$S_2(\rho) = a_4 + \frac{p_0}{\rho_0^2} (\rho - \rho_0) + \dots \quad (36)$$

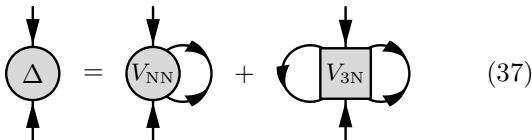
Here  $A$  is the nucleon number,  $a_V$  the binding energy of symmetric nuclear matter at saturation density,  $K$  is the incompressibility,  $a_4$  the symmetry energy and  $p_0$  the linear dependence of the symmetry energy.

Using the band of Fig. 8 over the density range  $0.13 \text{ fm}^{-3} < \rho < 0.19 \text{ fm}^{-3}$  with empirical values for the saturation point  $\rho_0 = 0.16 \text{ fm}^{-3}$ ,  $a_V = 16$  MeV and incompressibilities  $K = 190/240$  MeV (which are in the range of empirical values [36] and were obtained for the same interactions in Ref. [8]), we find in Table II that the symmetry energy ranges from  $a_4 = (30.4 - 33.6)$  MeV and the linear dependence of the symmetry energy from

$p_0 = (2.0 - 2.9) \text{ MeV fm}^{-3}$ . The value for  $p_0$  is practically independent of the values of  $K$ . As shown in Table II, the resulting range for the symmetry energy and its density dependence is set by the uncertainty of the dominant  $c_3$ . Compared to the empirical range  $a_4 = (25 - 35) \text{ MeV}$  [36], the microscopic range of  $\sim 3 \text{ MeV}$  is very useful and the comparison also suggests that smaller values in magnitude for  $c_3$  may be somewhat favored.

### F. $^1\text{S}_0$ pairing gap

Three-nucleon forces also impact superfluid pairing gaps or the anomalous self-energy. Here we will focus on the change of the neutron-neutron  $^1\text{S}_0$  pairing gap  $\Delta$  due to chiral 3N forces compared to the gap based on NN interactions. For simplicity, we neglect induced interactions and study the pairing gap at the BCS level. In this approximation, the contribution of 3N forces to the pairing interaction originates from two paired particles on the Fermi surface in back-to-back momentum states and the third particle is summed over occupied states in the superfluid BCS ground state. This means that the gap equation is given diagrammatically by



$$\Delta = V_{\text{NN}} + V_{\text{3N}} \quad (37)$$

The kinematics in  $V_{3\text{N}}$  is always  $P = 0$  for the interacting particle pair in the gap equation and therefore taking  $P = 0$  in  $\bar{V}_{3\text{N}}$  is exact in this case. The only approximation using  $\bar{V}_{3\text{N}}$  at the BCS level consists in having performed the sum over occupied states in the normal Fermi sea. However, the difference to summing over occupied states in the BCS state is of higher order in  $\Delta/\varepsilon_{\text{F}}$  ( $\varepsilon_{\text{F}} = k_{\text{F}}^2/(2m)$  being the Fermi energy), which is small in neutron matter especially at the densities where 3N forces are effective.

In the BCS approximation, the  $^1\text{S}_0$  superfluid gap  $\Delta(k)$  is obtained by solving the gap equation,

$$\Delta(k) = -\frac{1}{\pi} \int dp p^2 \frac{V_{^1\text{S}_0}^{(2)}(k, p) \Delta(p)}{\sqrt{(\varepsilon_{\text{p}} - \mu)^2 + \Delta^2(p)}}, \quad (38)$$

where the chemical potential  $\mu = \varepsilon_{k_{\text{F}}}$  at the BCS level and the pairing interaction is given by the two-body interaction including  $\bar{V}_{3\text{N}}$  in the  $^1\text{S}_0$  channel, so that  $V_{^1\text{S}_0}^{(2)} = V_{\text{low } k, ^1\text{S}_0} + \bar{V}_{3\text{N}, ^1\text{S}_0}/2$ . The gap equation including 3N forces, Eq. (38), can be derived explicitly by minimizing the expectation value of the Hamiltonian in the BCS state [37].

We consider two cases for the single-particle energies, a free spectrum  $\varepsilon_{\mathbf{k}} = k^2/(2m)$  and Hartree-Fock single-particle energies  $\varepsilon_{\mathbf{k}}^{(1)} = k^2/(2m) + \Sigma^{(1)}(k)$ , and solve the gap equation, Eq. (38), as in Ref. [22]. Our results for the neutron-neutron pairing gap on the Fermi

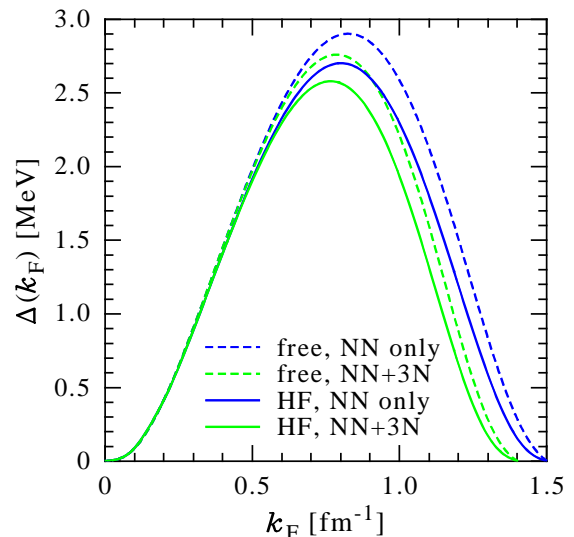


FIG. 10: (Color online) The neutron-neutron  $^1\text{S}_0$  superfluid pairing gap on the Fermi surface  $\Delta(k_{\text{F}})$  as a function of Fermi momentum  $k_{\text{F}}$ . The results are based on evolved  $\text{N}^3\text{LO}$  NN potentials and  $\text{N}^2\text{LO}$  3N forces with  $\Lambda/\Lambda_{3\text{NF}} = 2.0 \text{ fm}^{-1}$  using free and Hartree-Fock single-particle energies.

surface  $\Delta(k_{\text{F}})$  are presented in Fig. 10 as a function of the Fermi momentum. The inclusion of  $\text{N}^2\text{LO}$  3N forces leads to a reduction of the pairing gap for Fermi momenta  $k_{\text{F}} > 0.6 \text{ fm}^{-1}$ , as expected since the  $^1\text{S}_0$  channel of  $\bar{V}_{3\text{N}}$  is repulsive in Fig. 2. This reduction agrees qualitatively with results based on 3N potential models, see for example, Ref. [38]. While the impact of 3N forces seems small in Fig. 10, for the densities, where the gap is decreasing, the reduction due to 3N forces is significant. Figure 10 also shows that the effects of 3N forces relative to NN interactions is very similar for free and Hartree-Fock single-particle energies.

## IV. CONCLUSIONS AND OUTLOOK

In summary, we have shown that only the  $c_1$  and  $c_3$  terms of the long-range  $2\pi$ -exchange part of the leading chiral 3N forces contribute in neutron matter. Based on these parts and including all exchange terms, we derived density-dependent two-body interactions  $\bar{V}_{3\text{N}}$  for general momentum and spin configurations by summing the third particle over occupied states in the Fermi sea. The resulting  $\bar{V}_{3\text{N}}$  was found to be dominated by the repulsive central part. The comparison to the exact Hartree-Fock energy demonstrated that the  $P$  dependence is very weak and we have therefore taken  $P = 0$  in  $\bar{V}_{3\text{N}}$ . In addition, the partial-wave matrix elements of our full  $\bar{V}_{3\text{N}}$  approximately agree with the density-dependent two-body forces derived recently in the framework of in-medium chiral perturbation theory with certain approximations in Ref. [39].

The density-dependent two-body interactions  $\overline{V}_{3N}$  correspond to the normal-ordered two-body part of 3N forces and we stressed that there are different normal ordering or symmetry factors when  $\overline{V}_{3N}$  is used at the Hartree-Fock, one- or two-body level. Moreover, it is important that the summation of the third particle over occupied states is performed in the basis consistent with the one used in the many-body calculation.

We have presented the first results for neutron matter based on chiral EFT interactions and including N<sup>2</sup>LO 3N forces. The RG evolution of N<sup>3</sup>LO NN potentials to low momenta rendered the many-body calculation more controlled and our results for the energy suggest that neutron matter is perturbative at nuclear densities. This is based on small second-order contributions, self-energy corrections being negligible, and a generally weak cutoff dependence. We have found that N<sup>2</sup>LO 3N forces provide a repulsive contribution to the energy due to the repulsive central part in  $\overline{V}_{3N}$ . An important direction for future work is understanding the connection to the repulsive 3N contributions to the oxygen isotopes discovered in Ref. [40].

We have studied in detail the theoretical uncertainties of the neutron matter energy and found that the uncertainty in the  $c_3$  coefficient of 3N forces dominates compared to other many-body uncertainties. This resulted in

an energy band in Fig. 9. Other recent neutron matter calculations were found to lie within this band. Moreover, the energy band provides microscopic constraints for the symmetry energy and its density dependence, and thus for the neutron skin in <sup>208</sup>Pb [42]. Finally, we have obtained a significant reduction of the <sup>1</sup>S<sub>0</sub> superfluid pairing gap due to 3N forces for densities where the gap is decreasing. Our results show that chiral EFT and RG interactions can provide useful constraints for developing a universal density functional based on microscopic interactions [4, 5, 41].

### Acknowledgments

We thank S. K. Bogner and R. J. Furnstahl for useful discussions and are grateful to J. W. Holt for the helpful comparison of  $\overline{V}_{3N}$  partial-wave matrix elements. This work was supported in part by the Natural Sciences and Engineering Research Council of Canada (NSERC) and by the Helmholtz Alliance Program of the Helmholtz Association, contract HA216/EMMI “Extremes of Density and Temperature: Cosmic Matter in the Laboratory”. TRIUMF receives funding via a contribution through the National Research Council Canada.

- 
- [1] A. Schwenk and C. J. Pethick, Phys. Rev. Lett. **95**, 160401 (2005).
  - [2] A. Gezerlis and J. Carlson, Phys. Rev. C **77**, 032801 (2008).
  - [3] S. Giorgini, L. P. Pitaevskii and S. Stringari, Rev. Mod. Phys. **80**, 1215 (2008).
  - [4] S. K. Bogner, R. J. Furnstahl and L. Platter, Eur. Phys. J. A **39**, 219 (2009).
  - [5] M. Stoitsov, J. More, W. Nazarewicz, J. C. Pei, J. Sarich, N. Schunck, A. Staszczak and S. Wild, J. of Physics: Conf. Series **180**, 012082 (2009).
  - [6] J. M. Lattimer and M. Prakash, Astrophys. J. **550** (2001) 426.
  - [7] S. K. Bogner, A. Schwenk, R. J. Furnstahl and A. Nogga, Nucl. Phys. A **763**, 59 (2005).
  - [8] S. K. Bogner, R. J. Furnstahl, A. Nogga and A. Schwenk, arXiv:0903.3366 [nucl-th].
  - [9] E. Epelbaum, Prog. Part. Nucl. Phys. **57**, 654 (2006).
  - [10] E. Epelbaum, H.-W. Hammer and U.-G. Meißner, Rev. Mod. Phys. **81**, 1773 (2009).
  - [11] S. K. Bogner, T. T. S. Kuo and A. Schwenk, Phys. Rept. **386**, 1 (2003); S. K. Bogner, A. Schwenk, T. T. S. Kuo and G. E. Brown, nucl-th/0111042.
  - [12] S. K. Bogner, R. J. Furnstahl, S. Ramanan and A. Schwenk, Nucl. Phys. A **784**, 79 (2007).
  - [13] S. K. Bogner, R. J. Furnstahl, P. Maris, R. J. Perry, A. Schwenk and J. P. Vary, Nucl. Phys. A **801**, 21 (2008).
  - [14] S. Bacca, A. Schwenk, G. Hagen and T. Papenbrock, Eur. Phys. J. A **42**, 553 (2009).
  - [15] D. R. Entem and R. Machleidt, Phys. Rev. C **68**, 041001(R) (2003).
  - [16] E. Epelbaum, W. Glöckle and U.-G. Meißner, Nucl. Phys. A **747**, 362 (2005).
  - [17] U. van Kolck, Phys. Rev. C **49**, 2932 (1994).
  - [18] E. Epelbaum, A. Nogga, W. Glöckle, H. Kamada, U.-G. Meißner and H. Witała, Phys. Rev. C **66**, 064001 (2002).
  - [19] D. W. Batt and B. H. J. McKellar, Phys. Rev. C **11**, 614 (1974).
  - [20] S. A. Coon, N. D. Scadron, P. C. McNamee and B. R. Barrett, Nucl. Phys. A **317**, 242 (1979).
  - [21] P. F. Bedaque and U. van Kolck, Annu. Rev. Nucl. Part. Sci. **52**, 339 (2002).
  - [22] K. Hebeler, A. Schwenk and B. Friman, Phys. Lett. B **648**, 176 (2007).
  - [23] S. K. Bogner, R. J. Furnstahl, S. Ramanan and A. Schwenk, Nucl. Phys. A **773**, 203 (2006).
  - [24] A. Nogga, S. K. Bogner and A. Schwenk, Phys. Rev. C **70**, 061002(R) (2004).
  - [25] L. Tolos, B. Friman and A. Schwenk, Nucl. Phys. A **806**, 105 (2008).
  - [26] J. W. Negele and H. Orland, *Quantum Many-Particle Systems* (Advanced Book Classics, Westview Press, 1998).
  - [27] For normal ordering with 3N forces, see Eq. (2) in G. Hagen, T. Papenbrock, D. J. Dean, A. Schwenk, A. Nogga, M. Włoch and P. Piecuch, Phys. Rev. C **76**, 034302 (2007); or Sect. 4.3 in S. K. Bogner, R. J. Furnstahl and A. Schwenk, arXiv:0912.3688 [nucl-th].
  - [28] M. Baldo, I. Bombaci and G. F. Burgio, Astron. Astrophys. **328**, 274 (1997).
  - [29] W. Zuo, A. Lejeune, U. Lombardo and J. F. Mathiot, Nucl. Phys. A **706**, 418 (2002).

- [30] V. Soma and P. Bozek, Phys. Rev. C **78**, 054003 (2008).
- [31] W. Zuo, I. Bombaci and U. Lombardo, Phys. Rev. C **60**, 024605 (1999).
- [32] U.-G. Meißner, private communication (2007). We have enlarged the upper limit for  $c_3$  to include the value used in Ref. [15].
- [33] J. Carlson, J. Morales, V. R. Pandharipande and D. G. Ravenhall, Phys. Rev. C **68**, 025802 (2003).
- [34] A. Akmal, V. R. Pandharipande and D. G. Ravenhall, Phys. Rev. C **58**, 1804 (1998).
- [35] R. J. Furnstahl, Nucl. Phys. A **706**, 85 (2002).
- [36] A. W. Steiner, M. Prakash, J. M. Lattimer and P. J. Ellis, Phys. Rept. **411**, 325 (2005).
- [37] L. Yuan, Ph.D. thesis (Washington University, St. Louis, 2006).
- [38] W. Zuo, Z. H. Li, G. C. Lu, J. Q. Li, W. Scheid, U. Lombardo, H.-J. Schulze and C. W. Shen, Phys. Lett. B **595**, 44 (2004).
- [39] J. W. Holt, N. Kaiser and W. Weise, arXiv:0910.1249 [nucl-th].
- [40] T. Otsuka, T. Suzuki, J. D. Holt, A. Schwenk and Y. Akaishi, arXiv:0908.2607 [nucl-th].
- [41] N. Kaiser, S. Fritsch and W. Weise, Nucl. Phys. A **724**, 47 (2003).
- [42] K. Hebeler and A. Schwenk, in preparation.